Title	Probing lattice dynamics in ST12 phase germanium nanowires by Raman spectroscopy
Authors	Raha, Sreyan;Srivastava, Divya;Biswas, Subhajit;Garcia-Gil, Adrià;Karttunen, Antii J.;Holmes, Justin D.;Singha, Achintya
Publication date	2021-12-08
Original Citation	Raha, S., Srivastava, D., Biswas, S., Garcia-Gil, A., Karttunen, A. J., Holmes, J. D. and Singha, A. (2021) 'Probing lattice dynamics in ST12 phase germanium nanowires by Raman spectroscopy', Applied Physics Letters, 119, (7 pp). doi: 10.1063/5.0066744
Type of publication	Article (peer-reviewed)
Link to publisher's version	https://aip.scitation.org/doi/10.1063/5.0066744 - 10.1063/5.0066744
Rights	Published under an exclusive license by AIP Publishing. This article may be downloaded for personal use only. Any other use requires prior permission of the author and AIP Publishing. This article appeared in Appl. Phys. Lett. 119, 232105 (2021) and may be found at https://doi.org/10.1063/5.0066744
Download date	2024-04-23 07:12:36
Item downloaded from	https://hdl.handle.net/10468/12376

Probing lattice dynamics in ST12 phase germanium nanowire by Raman spectroscopy

Sreyan Raha,[1] Divya Srivastava,[2] Subhajit Biswas,[3] Adrià Garcia-Gil,[3] Antti J. Karttunen,[2] Justin D Holmes,[3] and Achintya Singha[1, a)]

[1)]*Department of Physics, Bose Institute, Acharya Prafulla Chandra road, Kolkata 700009, India*

[2)]*Department of Chemistry and Materials Science, Aalto University, P.O. Box 16100, FI-00076, Aalto, Finland*

[3)]*School of Chemistry & Advanced Materials and Bioengineering Research (AMBER) Centre, University College Cork, Cork T12 YN60, Ireland*

(Dated: 1 December 2021)

Germanium (Ge) plays a crucial role in setting up important functionalities for silicon-compatible photonics. Diamond cubic germanium is an extensively studied semiconductor, although its other exotic forms like BC8, ST8, ST12 phases may possess distinct electronic properties. We have fabricated stable ST12-Ge nanowires via a self-seeded bottom-up three phase growth in a confined supercritical toluene environment. Here we report on the direct evidence of the presence of ST12 phase by a combination of Raman spectroscopy and first-principles calculations using density functional theory. It is important to remark that the DFT calculation predicts all the Raman active optical phonon modes of $P4_32_1$ structure and it is in very good agreement with the experimental results. The phonon dynamics as a function of temperature is investigated through Raman measurements at temperatures varying from 80 to 300 K. First-order temperature coefficients for all the observed Raman modes are estimated from the linear temperature dependence of the phonon shifts. A complete set of isobaric Grüneisen parameters (γ_{ip}) is reported for all Raman modes of ST12-Ge nanowire and the values are lower compared to the same for Si, dc-Ge bulk and nanowire. These results have important implications for understanding thermal properties of ST12-Ge nanowire.

Group IV elements have drawn great attention because of their potential applications in present-day consumables and devices[1–6]. Germanium (Ge) is one of the widely used group IV materials for the development of photonics, nanoelectronics and optoelectronics[7–10]. Though the diamond cubic (dc) Ge is mostly studied and used, Ge can also be found in some other exotic forms which are potentially very useful in photovoltaics, transistors, superconducting devices[11–14]. These phases can be procured on the suitable tuning of thermodynamic condition especially pressure[15]. However, most of the phases are metastable and can only be realized under a definite decompression condition of compressed Ge[16–22]. Under pressure, dc-Ge undergoes a series of transformations. At 10-11 GPa it converts into metallic $\beta - Sn$ Ge, which transforms into orthorhombic *Imma* phase around 75 GPa and then simple hexagonal structure around 90 GPa[23–25]. Around 100 GPa, it transforms to a *Cmma* phase, which changes into *hcp* structure around 160-180 GPa. When *hcp* Ge is decompressed, it does not follow its previous path. Moreover, it forms various allotropes depending on the rate of pressure release. It is reported that on decompression Ge can take various structures such as BC8, R8, ST12[24,26–29]. $\beta - Sn$ phase readily transforms into BC8 phase and then hexagonal Ge on very fast release of pressure[16,25,28,30], while slow decompression results in metastable ST12 structure[17,18,31]. Some reports also suggest that metallic amorphous Ge, formed by pressure, can be transformed to both BC8[16,19,29] and ST12 phase[20] on depressurization.

Among all the Ge allotropes, ST12 is kinetically more sta-

ble at ambient conditions. It contains 12 atoms per unit cell in the space group $P4_32_12$ (D_4^8)[32] and possess distorted tetrahedral arrangement with atoms placed in five-fold, six-fold and seven-fold rings[32,33]. So, the electronic property of the ST-12 Ge is expected to be semiconducting and can be also realized as a superconductor at low temperature by doping[13,14]. Moreover, due to the stronger binding interaction of Li atoms within the ST12 Ge lattices, it shows higher Li intercalation compared to the dc-Ge and demonstrates as a promising candidate for energy storage applications[11]. Theoretical and experimental efforts have been devoted to explore the electronic band structure and thermal stability of the ST12-Ge[13,31,34,35]. However, studies on lattice dynamics which is responsible for thermal properties of a material, are limited. Malone and Cohen have calculated phonon dispersions for bulk ST12-Ge using LDA[13]. Raman scattering is among the most conventional and fundamental techniques for studying lattice dynamics of materials in an easy and nondestructive manner. The structural and vibrational properties of the various phases of Ge under pressure has been studied using Raman spectroscopy. Very recently, Zhao et al., reported optical phonon modes of bulk ST12-Ge via Raman analysis and calculation[32]. The reported results, however, are limited to the bulk system and no one has observed all the Raman active optical modes of ST12-Ge crystal. Downscaling the dimension of ST12-Ge to a nanometer regime may lead to potential functionality and device concepts. We are aware of few reports on nanocrystalline ST12-Ge fabricated through thermal annealing of amorphous nanoscale Ge[36], and evaporation[37,38]. But, no one synthesized the quasi one-dimensional nanostructures which are used as the building blocks for several technologies including electronics[39], optoelectronics[1,2], energy stor-
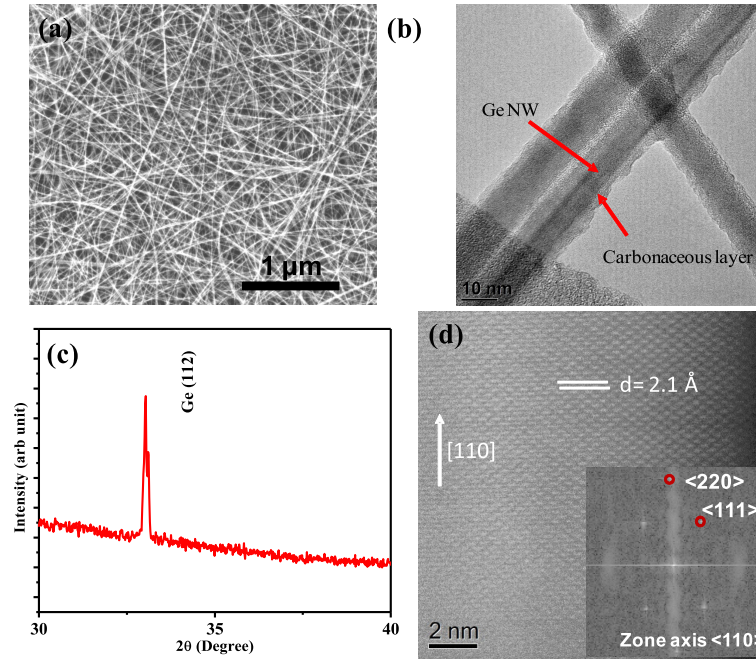

FIG. 1. (a) SEM micrographs of ST12-Ge NW. (b) Low magnification TEM image showing the uniform diameter nanowire formation with amorphous shell. (c) XRD pattern of the nanowire sample showing a ST12-Ge crystal structure obtained after subtracting the Si (100) substrate peaks. (d) Latticed-resolved HRTEM image and corresponding FFT (in the inset) of ST12-Ge nanowires.

age device[3,4,40,41] and sensor[5,6,42,43].

Here, we demonstrate the synthesis of ST12-Ge nanowires (NW). The phase and purity of the NW are confirmed from X-ray diffraction (XRD) and high-resolution transmission electron microscopy (HRTEM). We have conducted a systematic Raman study and observed almost all the Raman-active optical phonon modes. DFT calculations were also performed. Combining calculated Raman frequencies and their intensity with the experimental results enable us to clearly identify all the observed modes. Finally, temperature dependent Raman measurements have been performed on ST-12 Ge, allowing us to estimate first-order temperature coefficients and isobaric Grüneisen parameters.

ST12-Ge NW synthesis procedure and the methods used for characterization are given in supplementary material. Figure 1(a) and (b) show representative low magnification SEM image and high magnification TEM image of ST12-Ge NWs (Methods used for characterization, can be found in supplementary material). Figure 1(a) exhibit the formation of high yield of reticulated NWs which are several micrometers long. Ge NWs assembled together to form a uniform continuous Ge film over the Si substrates. SEM analysis become limited for accurate estimation of the morphological quality of the NW and the NW surface due to the reticulation of the NWs.Thus, detailed morphological analysis of the NWs is performed via TEM. Presence of an amorphous carbonaceous structures can be spotted along the Ge NW as an uneven coating (Figure 1(b)). The formation of the carbonaceous structure was confirmed via X-ray photoelectron spectroscopy (XPS), with the presence of Ge-C, C-C, C=C, C-O and CO_3 bonds in the C1s

spectrum (please see Figure S1 in supplementary material). The formation of the carbonaceous compound is aided by the decomposition of the Ge precursor (DPG) to form Ge adatoms and liberating very reactive phenyl groups[44]. The in-situ formation of Ge nanoparticle seed and the carboneceous compound on NW surface, and its interaction with the Ge is key for the formation of the ST-12 NW structure. We have delegated details of the growth mechanism of ST12-Ge NW to a different study as this paper is primarily focused on the Raman analysis of these structures. The diameter of Ge NWs was found to be uniform with an average diameter of 9.0 (± 1.4) nm.

XRD on the as-grown NW was performed to confirm the crystal structure and the phase purity of the NWs (Figure 1(c)). The pattern shows a sharp peak at 2θ of 33.29^o, after subtracting the reflection peaks from the Si pattern of the substrate. The XRD pattern matches well with the calculated and experimental XRD pattern of ST12-Ge (JCPDS No. 72-1089, $a = 5.93$Å and $c = 6.98$Å)[45,46]. We have assigned the peak in the XRD pattern to the reflection from the (112) plane as this is the closest match with the 2θ value. Peaks corresponding to dc-Ge were not observed in the XRD pattern. The single peak observed in the XRD corresponds to the strongest (112) reflection from the ST-12 Ge sample and associated with the crystallographic orientation of the one-dimensional NW. Due to the bulk crystalline nature of the sample, Zhao et al. have observed several diffraction peaks in their PXRD data associated with the different lattice planes of the ST-12 crystal[32]. HRTEM and Fast Fourier Transform (FFT) were used to further confirm the formation of ST12-Ge crystalline phase in the
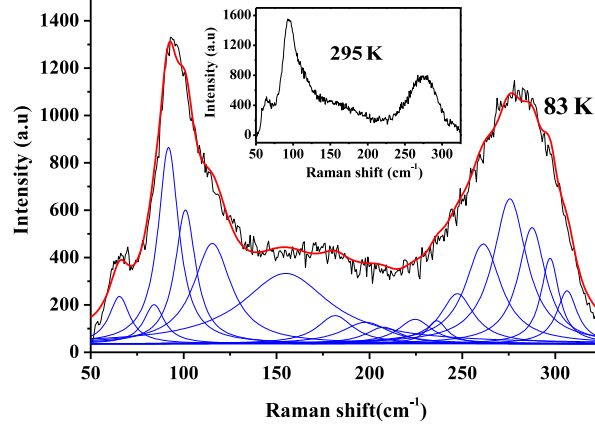
FIG. 2. Deconvoluted Raman spectrum of ST12-Ge NW measured at 83 K fitted with 17 Lorentzian functions. Inset shows the Raman spectrum of ST12-Ge NW at 295 K.
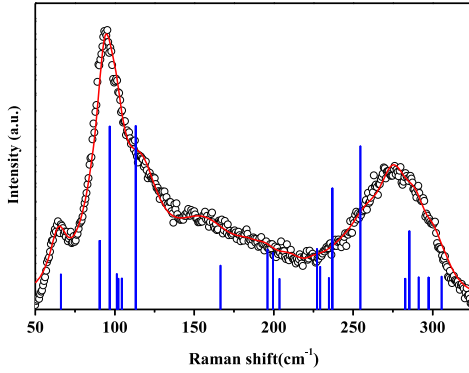

FIG. 3. Experimental Raman spectrum of ST12-Ge NW and calculated Raman modes (blue bars) with undefined FWHMs. Height of each bar is the measure of intensity of corresponding Raman mode.

Ge NWs and also verify the structural quality of the ST12-Ge NWs (Figure 1(d)). In general, NWs are single crystalline and free of any crystalline defects such as twin boundaries and stacking faults. HRTEM image recorded with <110> zone axis alignment, reveals an interplanar spacing (d) of 0.21 nm corresponding to (220) plane of the ST12-Ge crystal structure (JCPDS No. 72-1089). A hexagonal symmetry was observed in the FFT pattern where the spots are associated with the (111) and (220) planes (inset of Figure 1(d)) where (220) is the growth direction of the ST12-Ge NW.The Selected Area Electron Diffraction (SAED) observed from the single crystalline bulk structure (in Zhao et. al. paper[32]) shows multiple spot pattern from different crystalline planes. They have observed this from [310], [100], and [210] zone axis.

First-principles calculations using DFT have been per-

formed to study the vibrational properties of both ST12-Ge and dc-Ge. The details of computational method is given in supplementary material. The DFT-PBE0[47]/TZVP optimized lattice parameters are $a = b = 5.92$Å, $c = 7.03$Åfor ST12-Ge and $a = b = c = 5.70$Åfor dc-Ge, which are in good agreement with experimental lattice parameters $a = b = 5.93$Å, $c = 6.98$Åfor ST12-Ge[32] and $a = b = c = 5.66$Åfor dc-Ge[48], respectively. For ST12-Ge, there are 36 vibrational modes. Three are acoustic and thirty three are optical modes. The optical vibrational modes belong to the following irreducible representations: $\Gamma_{vib} = 4A_1 + 4A_2 + 5B_1 + 4B_2 + 8E$. A_1 and B_2 are totally-symmetric and totally-anti-symmetric phonon modes, respectively. E is doubly degenerate phonon modes. A_2 (B_1) is symmetric (anti-symmetric) with respect to principal axis of symmetry and anti-symmetric (symmetric) with respect to a C_2 axis. The modes A_2 and E are infrared-active mode whereas A_1, B_1, B_2 and E are Raman-active modes. Our DFT calculations predict 21 ($4A_1 + 5B_1 + 4B_2 + 8E$) Raman active optical modes, which is in accordance with group theoretical analysis of $P4_32_1$ structure[32] and previously reported DFT calculations[13]. This agreement is consequence of imposing space group constrain on crystal structure during optimization. The Raman frequency and the symmetry of the modes estimated from the calculation are presented in the second column of Table I. For comparison we have calculated Raman spectrum of dc-Ge which shows Raman active mode (E_{2g}) originates from a degenerate LO-TO phonon mode (see Figure S2 in supplementary material).

Figure 2 displays a typical Raman spectrum in 50-325 cm^{-1} range measured from the ST12-Ge NW sample at 83 K. A similar Raman spectrum measured from the same NW sample at room temperature is shown in the inset of Figure 2. Both the spectra show identical line shapes. However, a better resolution is observed in the spectrum recorded at low temperatures. In ST12-Ge NWs with average diameter 9 nm, the quantum confinement effect is very obvious. The confine-
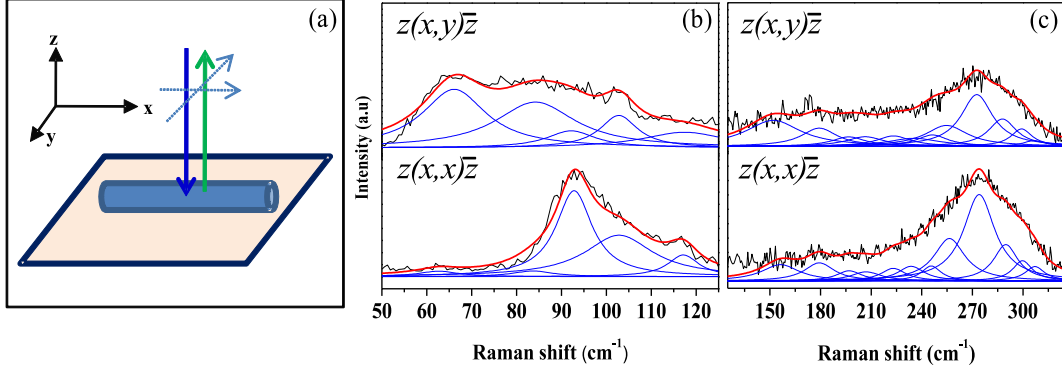
FIG. 4. (a) Illustration of the scattering geometry for polarized Raman measurements. Light is incident and scattered along z and $\bar{z}$ axis, respectively.The polarization of the light lies in the xy plane. (b), (c) Deconvoluted Raman spectra for two polarization configurations as labelled in the figure ranging from 50 to 125 cm^{-1} and 125 to 325 cm^{-1} respectively.
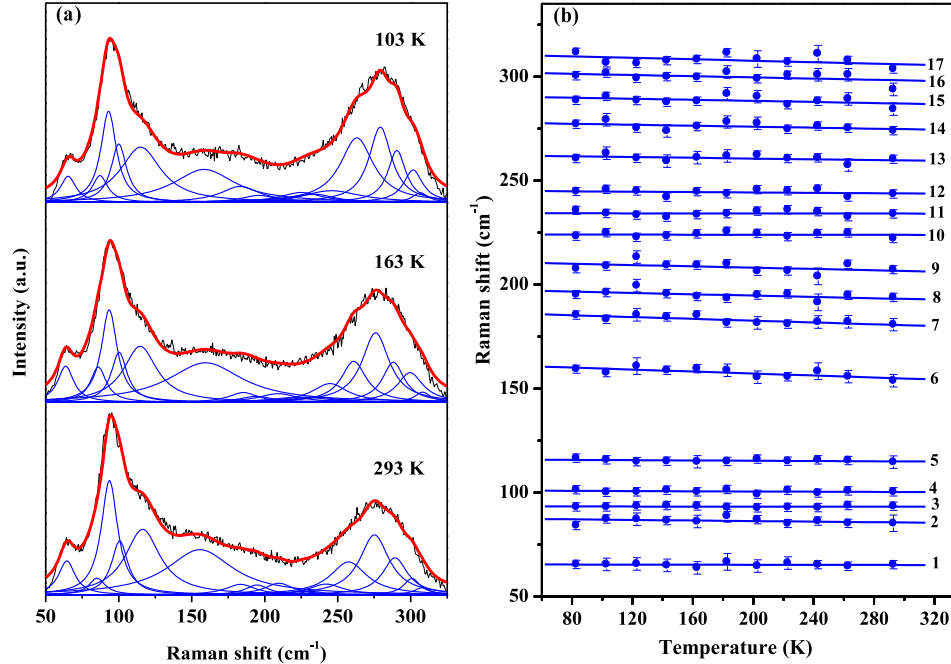

FIG. 5. (a) Raman spectra of ST12-Ge NW measured at 103, 163 and 293 K (scattered curves). The spectra are fitted with Lorentzian functions (blue curves). (b) Temperature dependence of the Raman peak position (scattered points) for all the observed modes. The solid lines represents the fit to equation (1).

ment of phonon relaxes the $q = 0$ selection rule in the Raman scattering and result in the change of phonon mode frequency and linewidth broadening. Moreover, the scattering of phonon in the low dimensional system provided additional linewidth broadening. Therefore, the Raman spectra are broad in the present work compared to the data reported by Zhao et al.[32]. Analysis of the spectra was performed very carefully. Out of 21 predicted modes from DFT calculation some modes are ex-

tremely weak and closely spaced [96.9 cm^{-1} (A1) and 101.3 cm^{-1} (E), 102.0 cm^{-1} (B2) and 104.5 cm^{-1} (B1), 234.7 cm^{-1} (E) and 237.0 cm^{-1} (B1), 282.7 cm^{-1} (E) and 285.4 cm^{-1} (A1)]. So, for deconvolution of the spectrum, we consider a single peak at the average position of two closed weak peaks. Therefore, to fit the experimental spectra we use 17 modes with the peak position, intensity, and width as free fitting parameters. The reference values of position are taken from the

TABLE I. Measured Raman frequency of ST12-Ge NW, calculated Raman frequency and symmetry of ST12-Ge and reported measured Raman modes of ST12-Ge from other works, first-order temperature co-efficient (β) and isobaric mode Grüneisen parameter (γ_{ip}).

Peak number	Calculated Raman frequency of ST12-Ge and symmetry (cm^{-1})	Experimentally measured Raman frequency (cm^{-1})	Reported Raman frequency of ST12-Ge from Zhao et al[32] (cm^{-1})	β_i (cm^{-1}K^{-1})	$\gamma_{ip} = -\frac{1}{\alpha\omega_i}\beta_i$
1	66.1(B_1)	65($\pm$2)	55	-0.00107($\pm$0.00049)	0.39($\pm$0.19)
2	90.5(E)	84($\pm$3)	85, 90	-0.00681($\pm$0.00071)	1.90($\pm$0.30)
3	96.9 (A_1), 101.3(E)	93($\pm$3)	100	-0.00052($\pm$0.00023)	0.13($\pm$0.06)
4	102.0(B_2), 104.5(B_1)	100($\pm$3)		-0.00256($\pm$0.00034)	0.60($\pm$0.10)
5	113.2(A_1)	116($\pm$3)		-0.00333($\pm$0.00051)	0.68($\pm$0.13)
6	166.5(E)	155($\pm$5)		-0.02328($\pm$0.00921)	3.56($\pm$1.49)
7	196.1(E)	183($\pm$5)	190	-0.02159($\pm$0.00263)	2.80($\pm$0.49)
8	199.5(A_1)	194($\pm$3)	200	-0.01587($\pm$0.00128)	1.93($\pm$0.20)
9	203.6(B_2)	209($\pm$4)		-0.01560($\pm$0.00241)	1.77($\pm$0.33)
10	227.3(B_1)	225($\pm$4)	210	-0.00071($\pm$0.00021)	0.07($\pm$0.02)
11	229.3(B_2)	232($\pm$2)	230	-0.00057($\pm$0.00023)	0.05($\pm$0.02)
12	234.7(E), 237.0(B_1)	242($\pm$4)		-0.00465($\pm$0.00025)	0.45($\pm$0.03)
13	254.5(E)	261($\pm$4)	257	-0.00886($\pm$0.00011)	0.81($\pm$0.02)
14	282.7(E), 285.4 (A_1)	275($\pm$5)	275	-0.01171($\pm$0.00602)	1.01($\pm$0.07)
15	291.3(E)	289($\pm$3)		-0.01288($\pm$0.00191)	1.06($\pm$0.16)
16	297.5(B_1)	300($\pm$4)		-0.01427($\pm$0.00607)	1.12($\pm$0.49)
17	305.7(B_2)	307($\pm$3)		-0.01756($\pm$0.00227)	1.35($\pm$0.18)

DFT calculation. The experimental spectrum is nicely fitted with 17 Lorentzian line shapes. The fitted data in the range 50-325 cm^{-1} is displayed in Figure 2 and their positions are presented in Table I. To obtain the error in the fitting we fit the spectrum five times and estimated error for peak position which are given in Table I.

Out of 17 observed Raman modes for ST12-Ge NWs, only some are previously reported[32] (see Table I). In this report of Raman analysis on ST12-Ge NW, the calculated Raman spectrum is almost fully matched with the experimental spectrum. The calculated intensities of the Raman modes also match nicely with the intensity pattern of the experimental spectrum as displayed in Figure 3, further adding credibility to our mode assignment.

To get the information about the Raman selection rule polarized Raman spectroscopy was performed on a single ST12 Ge NW transferred on a substrate. The measurements were performed in backscattering geometry. The light is incident on the NW along z-direction and scattered along $\bar{z}$-direction. The polarization of the incident light lies in xy plane. The experiment was carried out in two different configurations. According to the Porto notation, the Raman spectra are marked as $z(x,x)\bar{z}$ where the polarization of the incident and scattered light both are parallel to the x axis and $z(x,y)\bar{z}$ where the polarization of the incident and scattered light are in crossed polarization configuration. We have divided the measured spectra into two segments (Figure 4). The modes below 125 cm^{-1} show strong polarization sensitivity but the modes above 125 cm^{-1} exhibit nearly polarization-independent behaviour. The modes at 66 cm^{-1} (B$_1$ and 90.5 cm^{-1} (E) are allowed

in crossed polarization configuration [$z(x,y)\bar{z}$] whereas the modes around 100 cm^{-1} (A$_1$ and E) and 102 cm^{-1} (B$_1$ and B$_2$) are week in $z(x,y)\bar{z}$ configuration and become stronger in $z(x,x)\bar{z}$ scattering geometry.

Furthermore, to get greater insight into lattice dynamics, we have performed temperature dependent Raman study between 80 K and 300 K. Raman spectra measured at different temperatures are shown in Figure 5 (a). For a more accurate analysis of the temperature-dependent Raman results, we have fitted the spectra with the Lorentzian functions. The estimated peak positions which are plotted as a function of temperature are shown in Figure 5 (b). All the ST12-Ge phonon modes show a redshift with the increase in the temperature. The Raman peak shift with temperature is mainly caused by anharmonic phonon-phonon interaction and thermal expansion. In order to analyze the temperature dependent phonon softening, we have used a simplified phonon decay model, originated from Balkanski's approach[49].

$$\omega_T = \omega_0 + \beta T \qquad (1)$$

where ω_o is the Raman frequency at 0 K and β is the first-order temperature coefficient. In this model, the higher-order temperature coefficients have not been taken into account as they are not significant in the studied temperature range.

We fitted the experimental result with the expression (1) and obtained values of β are given in Table I. The β value for dc-Ge NW (-0.0147 cm^{-1}K^{-1}) has also been estimated from the data presented in the Figure S4(see supplementary material) and it is in good agreement with the previous work[50]. The estimated β values for most of the Raman modes of ST12-Ge

are lower than the same for dc-Ge. The observed differences in the β indicates that phonon anharmonicity caused by the scattering is lower in the ST12-Ge NW compared to the dc-Ge NW[51].

Grüneisen parameter (γ) is an important thermo elastic value of solid which describes the changes of unit cell volume caused by temperature and pressure. This parameter relates the property of a material to its vibrational energy and indicates the anharmonic effects on the phonon spectrum under temperature and pressure. The isobaric mode Grüneisen parameter (γ_{ip}) is related to the β by means of the equation[52]:

$$\gamma_{ip} = -\frac{1}{\alpha \omega_i}\beta_i \qquad (2)$$

where, ω_i is the Raman frequency of the i_{th} phonon mode, α is the thermal expansion coefficient.

To calculate γ_{ip}, we have taken the value of α for ST12-Ge from the Ref.[53]. Using equation (2), a complete set of γ_{ip} calculated from experimentally obtained β_i values for the entire observed optical phonon modes is reported in the last column of Table I. To compare the present results with the dc-Ge, we have estimated γ_{ip} for dc-Ge bulk and NW from the temperature dependent Raman data which are presented in Figure S3 and Figure S4 in supplementary material, respectively. The obtained γ_{ip} for dc-Ge bulk and NW are 11.92 and 8.25 respectively, which are higher than the γ_{ip} of ST12-Ge NW (3.56). It is to be noted that the γ_{ip} values for both the NWs are lower than the same for bulk. With the decrease of the size of nanostructured materials the bond length increases[54], which reduces the lattice interaction as well and lower the lattice vibration. As a result, less anharmonicity vibration gives lower values of the Grüneisen parameter.[55,56] High γ_{ip} value indicates lower thermal conductivity (k)[51]. Hence, it is expected that the ST12-Ge NWs show low optical phonon scattering and high electrical and thermal conductivity compared to dc-Ge bulk and NW. Moreover, γ_{ip} values of the ST12-Ge are also lower than the γ_{ip} of silicon (7.00)[57]. Therefore, the result implies that the ST12-Ge NW can be useful as a potential candidate for thermal and electrical conductive material.

In summary, we have fabricated ST12-Ge NWs and confirmed the existence of this uncommon allotrope by XRD, HRTEM and Raman study. In particular, we have performed detailed Raman spectroscopy and DFT analysis to pinpoint the ST12 phase of the nanostructure, and to explore the phonon dynamics in this material. The experimentally measured Raman spectra are in agreement with the DFT calculations. Furthermore, the temperature dependent lattice dynamics of ST12-Ge NWs is investigated through temperature dependent Raman study. From the temperature dependent study, we have estimated first-order temperature coefficients and isobaric Grüneisen parameter for all the observed modes of ST12-Ge and the values are lower than the Si, dc-Ge bulk and NW. Thus our study not only provides the fundamental information that are important for technological applications of ST12-Ge but, also attracts attention for further investigations on the role of dimension in polymorphism and in the thermal/vibrational properties of low-dimensional polymorphism of Ge, Si and other semiconductors.

Supplementary material

See supplementary material for methods of nanowire synthesis, characterization, computational methods, XPS of ST12-Ge NW, calculated Raman spectrum of dc-Ge, temperature dependent Raman study of bulk dc-Ge and dc-Ge NW.

DATA AVAILABILITY

The data that support the findings of this study are available from the corresponding author upon reasonable request.

REFERENCES

[1] P. Staudinger, M. Sistani, J. Greil, E. Bertagnolli, and A. Lugstein, "Ultrascaled germanium nanowires for highly sensitive photodetection at the quantum ballistic limit," Nano Lett. **18**, 5030–5035 (2018).

[2] L. N. Quan, J. Kang, C.-Z. Ning, and P. Yang, "Nanowires for photonics," Chem. Rev. **119**, 9153–9169 (2019).

[3] C. K. Chan, H. Peng, G. Liu, K. McIlwrath, X. F. Zhang, R. A. Huggins, and Y. Cui, "High-performance lithium battery anodes using silicon nanowires," Nat. Nanotech. **3**, 31–35 (2008).

[4] A. M. Chockla, K. C. Klavetter, C. B. Mullins, and B. A. Korgel, "Solution-grown germanium nanowire anodes for lithium-ion batteries," ACS Appl. Mater. Interfaces **4**, 4658–4664 (2012).

[5] N. Shehada, J. C. Cancill, J. S. Torrecilla, E. S. Pariente, G. Brönstrup, S. Christiansen, D. W. Johnson, M. Leja, M. P. A. Davies, O. Liran, N. Peled, and H. Haick, "Silicon nanowire sensors enable diagnosis of patients via exhaled breath," ACS Nano **10**, 7047–7057 (2016).

[6] L. Hrachowinaa, G. Domènech-Gil, A. Pardo, M. S. Seifner, I. Gràcia, C. Cané, A. Romano-Rodríguez, and S. Barth, "Site-specific growth and in situ integration of different nanowire material networks on a single chip: Toward a nanowire-based electronic nose for gas detection," ACS Sens. **3**, 727–734 (2018).

[7] D. Marris-Morini, V. Vakarin, J. M. Ramirez, Q. Liu, A. Ballabio, J. Frigerio, M. Montesinos, C. Alonso-Ramos, X. Le, S. Serna, D. Benedikovic, D. Chrastina, L. Vivien, and G. Isella, "Germanium-based integrated photonics from near- to mid-infrared applications," Nanophotonics **7**, 1781–1793 (2018).

[8] S. Liao, N.-N. Feng, D. Feng, P. Dong, R. Shafiiha, C.-C. Kung, H. Liang, W. Qian, Y. Liu, J. Fong, J. E. Cunningham, Y. Luo, and M. Asghari, "36 ghz submicron silicon waveguide germanium photodetector," Optics Express **19**, 10967–10972 (2011).

[9] C. Monmeyran, I. F. Crowe, R. M. Gwilliam, J. Michel, L. C. Kimerling, and A. M. Agarwal, "Strategies for increased donor electrical activity in germanium (opto-) electronic materials: a review," International Materials Reviews **62**, 334–347 (2016).

[10] Z. Qi, H. Sun, M. Luo, Y. Jung, and D. Nam, "Strained germanium nanowire optoelectronic devices for photonic-integrated circuits," Journal of Physics: Condensed Matter **30**, 334004 (2018).

[11] Y. J. Cho, H. S. Im, H. S. Kim, Y. Myung, S. H. Back, Y. R. Lim, C. S. Jung, D. M. Jang, J. Park, E. H. Cha, W. I. Cho, F. Shojaei, and H. S. Kang, "Tetragonal phase germanium nanocrystals in lithium ion batteries," ACS Nano **7**, 9075–9084 (2013).

[12] Y. Ikoma, T. Toyota, Y. Ejiri, K. Saito, Q. Guo, and Z. Horita, "Allotropic phase transformation and photoluminescence of germanium nanograins processed by high-pressure torsion," J. Mater. Sci. **51**, 138–143 (2016).

[13] B. D. Malone and M. L. Cohen, "Electronic structure, equation of state, and

lattice dynamics of low-pressure ge polymorphs," Phys. Rev. B **86**, 054101 (2012).

[14] D. Selli, I. A. Baburin, R. Martoňák, and S. Leoni, "Novel metastable metallic and semiconducting germaniums," Sci. Rep. **3** (2013), 10.1038/srep01466.

[15] A. Grüttner, R. Nesper, and H. G. v. Schnering, "Novel metastable germanium modifications allo-ge and 4h-ge from li_7ge_{12}," Angew. Chem. Int. Ed. Engl. **21**, 912–913 (1982).

[16] S. Minomura, "Pressure-induced transitions in amorphous silicon and germanium," J. Phys. Colloq. **42**, C4–181–C4–188 (1981).

[17] S. B. Qadri, E. F. Skelton, and A. W. Webb, "High pressure studies of ge using synchrotron radiation," J. Appl. Phys. **54**, 3609–3611 (1983).

[18] F. P. Bundy and J. S. Kasper, "A new dense form of solid germanium," Science **139**, 340–341 (1963).

[19] M. Imai, T. Mitamura, K. Yaoita, and K. Tsuji, "Pressure-induced phase transition of crystalline and amorphous silicon and germanium at low temperatures," High Press. Res. **15**, 167–189 (1996).

[20] F. Coppari, J. C. Chervin, A. Congeduti, M. Lazzeri, A. Polian, E. Principi, and A. D. Cicco, "Pressure-induced phase transitions in amorphous and metastable crystalline germanium by raman scattering, x-ray spectroscopy, and ab initio calculations," Phys. Rev. B **424**, 839–846 (2009).

[21] J. V. Zaikina, E. Muthuswamy, K. I. Lilova, Z. M. Gibbs, M. Zeilinger, G. J. Snyder, T. F. Fässler, A. Navrotsky, and S. M. Kauzlarich, "Thermochemistry, morphology, and optical characterization of germanium allotropes," Chem. Mater. **26**, 3263–3271 (2014).

[22] S. Sato, S. Nozaki, and H. Morisaki, "Tetragonal germanium films deposited by the cluster-beam evaporation technique," Appl. Phys. Lett. **66**, 3176 (1995).

[23] R. Nelmes, H. Liu, S. Belmonte, J. Loveday, M. McMahon, D. Allan, D. Häusermann, and M. Hanfland, "Imma phase of germanium at b80 gpa." Phys. Rev. B **53**, R2907–R2909 (R) (1996).

[24] X. Chen, C. Zhang, Y. Meng, R. Zhang, H. Lin, V. Struzhkin, and H. Mao, "-tin→imma→sh phase transitions of germanium," Phys. Rev. Lett. **106**, 135502 (2011).

[25] A. G. Lyapin, V. V. Brazhkin, S. V. Popova, and A. V. Sapeliki, "Nonequilibrium phase transformations in diamond and zincblende semiconductors under high pressure," Phys. Stat. Solid. B **198**, 481–490 (1996).

[26] Y. K. Vohra, K. E. Brister, S. Desgreniers, A. L. Ruoff, K. J. Chang, and M. L. Cohen, "Phase-transition studies of germanium to 1.25 mbar," Phys. Rev. Lett. **56**, 1944–1947 (1986).

[27] K. Takemura, U. Schwarz, K. Syassen, M. Hanfland, N. E. Christensen, D. L. Novikov, and I. Loa, "High-pressure cmca and hcp phases of germanium," Phys. Rev. B **62**, R10603(R) (2000).

[28] C. H. Bates, F. Dachille, and R. Roy, "High-pressure transitions of germanium and a new high-pressure form of germanium," Science **147**, 860–862 (1965).

[29] B. C. Johnson, B. Haberl, S. Deshmukh, D. Brad Malone, M. L. Cohen, J. C. McCallum, J. S. Williams, and J. E. Bradby, "Evidence for the r8 phase of germanium," Phys. Rev. Lett. **110**, 085502 (2013).

[30] R. J. Nelmes, M. I. McMahon, N. G. Wright, D. R. Allan, and J. S. Loveday, "Stability and crystal structure of bc8 germanium," Phys. Rev. B **96**, 9883(R) (1993).

[31] J. D. Joannopoulos and M. L. Cohen, "Electronic properties of complex crystalline and amorphous phases of ge and si. i. density of states and band structures," Phys. Rev. B **7**, 2644–2657 (1973).

[32] Z. Zhao, H. Zhang, D. Y. Kim, W. Hu, E. S. Bullock, and T. A. Strobel, "Properties of the exotic metastable st12 germanium allotrope," Nature Communication **8** (2017), 10.1038/ncomms13909.

[33] L. Q. Hutson, B. C. Johnson, B. Haberl, S. Wong, J. S. Williams, and J. E. Bradby, "Thermal stability of simple tetragonal and hexagonal germanium," Journal of Applied Physics **122**, 175108 (2017).

[34] M. A. and R. J. Needs, "First-principles calculations of the structural properties, stability, and band structure of complex tetrahedral phases of germanium: St12 and bc8," Phys. Rev. B **48**, 17010–17017 (1993).

[35] M. Shishkin and G. Kresse, "Self-consistent gw calculations for semiconductors and insulators," Phys. Rev. B **75**, 235102 (2007).

[36] S. J. Kim, O. K. Quy, L.-S. Chang, E. A. Stach, C. A. Handwerker, and A. Wei, "Formation of the st12 phase in nanocrystalline ge at ambient pressure," J. Mater. Chem. **20**, 331–337 (2010).

[37] S. Sato, S. Nazaki, and H. Morisaki, "Density of states of the tetragonal-phase germanium nanocrystals using x-ray photoelectron spectroscopy," Appl. Phys. Lett. **72**, 2460–2462 (1998).

[38] Y. Saito, "Crystal structure and habit of sillicon and germanium particles grown in argon gas," Journal of Crystal Growth **47**, 61–72 (1979).

[39] C. Jia, Z. Lin, Y. Huang, and X. Duan, "Nanowire electronics: From nanoscale to macroscale," Chem. Rev. **119**, 9074–9135 (2019).

[40] C. K. Chan, X. F. Zhang, and Y. Cui, "High capacity li ion battery anodes using ge nanowires," Nano Lett. **8**, 307–309 (2008).

[41] T. Kennedy, E. Mullane, H. Geaney, M. Osiak, C. O. Dwyer, and K. M. Ryan, "High-performance germanium nanowire-based lithium-ion battery anodes extending over 1000 cycles through in situ formation of a continuous porous network," Nano Lett. **14**, 716–123 (2014).

[42] F. Shen, J. Wang, Z. Xu, Y. Wu, Q. Chen, L. Xiaoguang, X. Jie, L. Li, M. Yao, X. Guo, and T. Zhu, "Rapid flu diagnosis using silicon nanowire sensor," Nano Lett. **12**, 3722–3730 (2012).

[43] S. Barth, R. Jimenez-Diaz, J. Samà, J. D. Prades, I. Gracia, J. Santander, C. Canec, and A. Romano-Rodriguez, "Localized growth and in situ integration of nanowires for device applications," Chem. Commun. **48**, 4734–4736 (2012).

[44] A. M. Chockla and B. A. Korgel, "Seeded germanium nanowire synthesis in solution," J. Mater. Chem. **19**, 996–1001 (2009).

[45] J. S. Kasper and S. M. Richards, "The crystal structures of new forms of silicon and germanium," Acta Crystallogr. **17**, 752–755 (1964).

[46] S. Bao, D. Kim, C. Onwukaeme, S. Gupta, K. Saraswat, K. H. Lee, Y. Kim, D. Min, Y. Jung, H. Qiu, H. Wang, E. A. Fitzgerald, C. T. Seng, and D. Nam, "Low-threshold optically pumped lasing in highly strained germanium nanowires," Nat Commun **8** (2017), https://doi.org/10.1038/s41467-017-02026-w.

[47] C. Adamo and V. Barone, "Toward reliable density functional methods without adjustable parameters: The pbe0 model," The Journal of Chemical Physics **110**, 6158–6170 (1999).

[48] A. S. Cooper, "Precise lattice constants of germanium, aluminum, gallium arsenide, uranium, sulphur, quartz and sapphire," Acta Crystallographica **15**, 578–582 (1962).

[49] M. Balkanski, R. F. Wallis, and E. Haro, "Anharmonic effects in light scattering due to optical phonons in silicon," Phys. Rev. B **28**, 1928–1934 (1983).

[50] D. Majumdar, S. Biswas, T. Ghoshal, J. D. Holmes, and A. Singha, "Probing thermal flux in twinned ge nanowires through raman spectroscopy," ACS Appl. Mater. Interfaces **4**, 24679–24685 (2015).

[51] A. Cassidy, N. Tsud, S. Bercha, V. Feyer, K. C. Prince, and O. Plekan, "Adsorption of 5-fluorouracil on au(111) and cu(111) surfaces," AIP Advances **9**, 085318 (2019).

[52] R. Singha, S. Samanta, S. Chatterjee, A. Pariari, D. Majumdar, B. Satpati, L. Wang, A. Singha, and P. Mandal, "Probing lattice dynamics and electron-phonon coupling in the topological nodal-line semimetal zrsis," Phys. Rev. B **97**, 094112 (2018).

[53] A. D. Cicco, A. C. Frasini, M. Minicucci, E. Principi, J. Itiè, and P. Munsch, "High-pressure and high-temperature study of phase transitions in solid germanium," physica status solidi (b) **240(1)**, 19–28 (2003).

[54] M. Omar, "Models for mean bonding length, melting point and lattice thermal expansion of nanoparticle materials," Materials Research Bulletin **47**, 3518–3522 (2012).

[55] S. Mamand, M. Omar, and A. Muhammad, "Nanoscale size dependence parameters on lattice thermal conductivity of wurtzite gan nanowires," Materials Research Bulletin **47**, 1264–1272 (2012).

[56] M. Omar and H. Taha, "Lattice dislocation in si nanowires," Physica B: Condensed Matter **404**, 5203–5206 (2009).

[57] D. S. Kim, H. L. Smith, J. L. Niedziela, C. W. Li, D. L. Abernathy, and B. Fultz, "Phonon anharmonicity in silicon from 100 to 1500 k," Phys. Rev. B **91**, 014307 (2015).